Pharmaceutical Research, Vol. 23, No. 8, August 2006 (© 2006)
DOI: 10.1007/s11095-006-9043-0

Research Paper

The Role of the VPS4A-Exosome Pathway in the Intrinsic Egress Route of a DNA-Binding Anticancer Drug

Vivien Y. Chen,[1] Maria M. Posada,[1] Levi L. Blazer,[1] Tong Zhao,[1] and Gus R. Rosania[1,2]

Received March 6, 2006; accepted April 18, 2006

Purpose. This study investigates the subcellular pharmacokinetics of drug efflux in cancer cells and explores the role of the multivesicular body (MVB) in facilitating efflux of doxorubicin, a widely used DNA-targeting anticancer agent, from the nucleus.
Methods. Human erythroleukemic K562 cells were pulsed with doxorubicin and then chased in drug-free media to allow for efflux. Microscopy and biochemical techniques were used to visualize the subcellular localization of the drug and measure drug content and distribution during the efflux period. To explore the role of the MVB in doxorubicin efflux, K562 cells were transfected with dominant negative mutant forms of VPS4a–GFP chimeras.
Results. Although the intracellular concentration of drug exceeds the extracellular concentration, nuclear efflux of doxorubicin occurs in living cells at a faster rate than doxorubicin unbinding from isolated nuclei into drug-free buffer. In cells expressing dominant negative VPS4a, doxorubicin accumulates in VPS4a-positive vesicles and drug sequestration is inhibited, directly implicating the MVB pathway in the egress route of doxorubicin in this cell type.
Conclusions. Cellular membranes are a component of the doxorubicin efflux mechanism in K562 cells. Dominant-negative GFP chimeric mutants can be used to elucidate the role of specific membrane trafficking pathways in subcellular drug transport routes.

KEY WORDS: cancer; doxorubicin; exosome; multivesicular body; nuclear efflux; subcellular transport; VPS4.

INTRODUCTION

Understanding drug transport mechanisms in tumor cells is crucial for developing anticancer agents with increased efficacy. Drug transport mechanisms are involved in multidrug resistance (MDR). MDR can be acquired or intrinsic: acquired MDR is due to mutations that confer cellular resistance to cytotoxic agents; intrinsic MDR is due to cell type-dependent and epigenetic differences in cellular responsiveness to chemotherapeutic agents (1). Upon exposure to chemotherapeutic agents, surviving resistant cells become the dominant cell population through clonal expansion. As a consequence, both intrinsic and acquired MDR mechanisms can conspire to render tumors refractory to treatment.

MDR is often associated with increased expression and activity of drug transporters that facilitate translocation of small molecule drugs across the plasma membrane (2). However, the actual MDR mechanism is multifactorial, with several different pathways acting together to promote cell survival upon exposure to cytotoxic agents (3). For example, in addition to their localization at the plasma membrane, drug transporters are also present in the membranes of cytoplasmic vesicles (4–6). Here, they can facilitate drug sequestration away from their site of action.

Doxorubicin is a clinically useful anticancer agent whose efficacy is often compromised by MDR mechanisms. Doxorubicin intercalates into nuclear DNA and prevents the repair of strand breaks by interfering with the activity of topoisomerase II, a DNA-unwinding enzyme (7). Doxorubicin is a substrate for drug transporters such as P-glycoprotein and Multidrug Resistance Protein 1 (8,9). Doxorubicin also accumulates in acidic cytoplasmic vesicles of cancer cells by active and passive transport mechanisms (10). The intrinsic fluorescence of doxorubicin and related anthracycline drugs have made them useful for studies of drug localization in resistant and sensitive cells (11–13).

As a hypothesis, the multivesicular body (MVB) could be involved in efflux of doxorubicin from its nuclear site-of-action. This hypothesis can be tested using K562 human erythroleukemic cells as an experimental model. K562 cells exhibit a significant level of intrinsic resistance to various anticancer agents, yet have low expression of known doxorubicin efflux transporters (14). K562 cells have an active and

[1] Department of Pharmaceutical Sciences, University of Michigan College of Pharmacy, 428 Church St., Ann Arbor, Michigan 48109, USA.
[2] To whom correspondence should be addressed. (e-mail: grosania@umich.edu)

ABBREVIATIONS: MDR, multidrug resistance; MVB, multivesicular body; VPS4a, vacuolar protein sorting 4a; GFP, green fluorescent protein; HEPES, 4-2-hydroxyethyl-1-piperazine-ethanesulfonic acid; EGTA, ethyleneglycol-bis-(β-aminoethylether)-N, N, N′, N′-tetraacetic acid; EDTA, ethylenediamine-tetraacetic acid; ER, endoplasmic reticulum.

well-characterized endocytic trafficking pathway with prominent MVBs (15). In these cells, the intralumenal vesicles of MVBs are released extracellularly as exosomes through fusion of MVBs with the plasma membrane (16,17). MVBs are acidic organelles, as are lysosomes.

Doxorubicin is a weak base with a pKa near neutrality that is prone to accumulating in acidic organelles as a result of pH-dependent ion trapping and membrane binding (18). Treatments that abolish the pH gradient result in drug efflux from acidic vesicles into the nucleus (10). In drug-resistant ovarian cancer cells, the anticancer drug cisplatin traffics to the extracellular medium via the MVB-exosomal pathway (19). Exosomes from drug-resistant ovarian cancer cells export more drug than from sensitive cells (19), suggesting that the intrinsic MVB-exosomal transport pathway may be upregulated in cells with the acquired MDR phenotype. Like cisplatin, doxorubicin could be released in complex with exosome-like membrane vesicles shed by cancer cells into extracellular medium (20).

Vacuolar Protein Sorting 4a (VPS4a) is a protein involved in the budding of exosomes and is essential for MVB formation (21,22). Transfection of cells with dominant negative VPS4a inhibits MVB-dependent membrane traffic (23–25). By transfecting K562 cells with VPS4a dominant-negative constructs, we explored how the MVB-exosome membrane trafficking mechanism is involved in doxorubicin's nuclear egress route.

MATERIALS AND METHODS

Cell Culture

K562 cells (ATCC, Manassas, VA) were maintained in tissue culture medium (RPMI supplemented with 10% FBS and 1% penicillin/streptomycin at 37°C with 5% CO_2). All experiments were done with cells in logarithmic growth phase ($0.2 - 1 \times 10^6$ cells/ml).

Efflux Experiments

Cells were pulsed with 100 μM doxorubicin (Bedford Laboratories, Bedford, OH) in RPMI for 2 h, unless indicated otherwise. Cells were washed twice with fresh tissue culture medium and chased in drug-free tissue culture medium for 0 to 8 h.

Microscopy

Cell suspensions (100 μl) were transferred to glass-bottom 96-well plates (Greiner Bio-One, Longwood, FL). Using a Nikon 2000S inverted microscope and 100× oil immersion objective for epifluorescence microscopy, images were acquired with a CCD camera (Roper Scientific, Tucson, AZ) with the standard epifluorescence mercury bulb illumination and a triple-pass DAPI/FITC/Texas Red beamsplitter/emission filter combination (Chroma Technology, Rockingham, VT). Doxorubicin (red emission) and GFP (green emission) were simultaneously visualized using the FITC excitation filter. For confocal microscopy, cells were monitored with an Olympus FV-500 microscope using a 100× oil immersion objective. An Argon laser (488 nm) illumination was used to acquire images of GFP, and a HeNe Green laser (543 nm) illumination was used to acquire images of doxorubicin, in two separate detection channels. Quantitative image analysis was performed with Metamorph software (Molecular Devices Corporation, Sunnyvale, CA). For electron microscopy, K562 cells were washed twice with serum-free media, incubated at 37°C with 2.5% glutaraldehyde in 0.1 M Sorensen's buffer at pH 7.4 for 30 min, and washed twice with 0.1 M Sorensen's buffer. Cells were fixed with 1% osmium tetroxide in 0.1 M Sorensen's buffer for 15 min at 4°C and washed three times with ddH_20. Uranyl acetate was added for a final concentration of 8%, and then cells were incubated for 1 h at room temperature. The sample was dehydrated in a graded ethanol:water series (50, 70, 90 and 100%) for 5 min each, and then infiltrated in Epon resin (Resolution Performance Products, Houston, TX) and polymerized at 60°C for 24 h. The stained cells were visualized and photographed with a Phillips CM/100 transmission electron microscope at magnifications from 3,600 to 130,000×. For all microscopy experiments, more than 20 cells were photographed for each experimental condition, and cells selected to be representative of their respective groups were included in the figures.

Image Processing

For epifluorescence microscope images, gamma was adjusted to 1.0 (linear signal-intensity relationship), and contrast was adjusted so that the maximum pixel signal was 256 (white) and background was 0 (black). For confocal microscopy, green and red channels were independently adjusted based on the amount of labeling of each cell, so as to best visualize the localization of GFP and doxorubicin signal in the cytoplasm. RGB color overlays were created with Adobe Photoshop from separate greyscale images, with the doxorubicin image in the R channel; GFP image in the G; and black fill in the B.

Doxorubicin Mass Measurements

To measure doxorubicin content, cells were incubated in a solution of 1% Triton in water. As observed using fluorescence microscopy, Triton X-100 treatment removed doxorubicin fluorescence from cytoplasmic structures, with any remaining doxorubicin fluorescence in association with nuclei. Following extraction, 100 μl samples containing 4 to 6×10^5 cells were transferred to individual wells in 96-well plates, and data was acquired with a Typhoon 9200 fluorescence scanner (Amersham Biosciences, Piscataway, NJ). Doxorubicin fluorescence was captured with green laser illumination (535 nm) and the 580 BP 30 emission filter on the instrument. To normalize for cell number, the nucleic acid stain Syto 63 (Molecular Probes, Eugene, OR) was added to each well at the concentrations recommended by the manufacturer, and imaged using red laser illumination (633 nm) and the 670 BP 30 emission filter. The 16-bit plate image data files were analyzed with Metamorph software. Doxorubicin mass in each well was calculated using a standard curve. The total number of cells in each well was calculated using standard curves made by varying numbers of cells stained with Syto. In each well, dividing the total mass of

doxorubicin by the number of nuclei yielded the mass of doxorubicin per cell. In validation experiments, we established that the integrated fluorescence intensity and total doxorubicin mass exhibited a linear relationship across the range of experimental measurements, and that measurements were comparable before and after digesting the DNA and proteins in the samples using DNase I and proteinase K. To confirm that total doxorubicin mass and fluorescence were conserved during the time course of the experiment, two separate measurements were performed: 1) measuring the mass of doxorubicin released from the cells into the surrounding media and 2) measuring the mass of doxorubicin in the cells. These two measurements corresponded to each other as expected from mass balance, with the drug lost from cells being equivalent to the doxorubicin gained in the extracellular medium (data not shown).

Compartmental Analysis

The mass of drug in different subcellular compartments (total, membrane, aqueous, and nuclear doxorubicin) was defined by measuring the mass of drug in different subcellular fractions following biochemical extractions. For quantifying the mass of drug associated with cell nuclei, membrane and freely soluble doxorubicin were extracted by incubating cells in 1% Triton in intracellular buffer (30 mM HEPES, 10 mM EGTA, 0.5 mM EDTA, 5 mM magnesium sulfate and 33 mM potassium acetate; pH 7.4) for 15 min. Nuclear pellets were isolated after centrifugation at 1,000 × g for 10 min, with aqueous and membrane doxorubicin fractions remaining in the supernatant. The nuclear pellet was checked using fluorescence microscopy to confirm that most (>95%) of the cells had been permeabilized. Nuclear pellets were washed twice and resuspended in buffer by vortexing. Nuclear doxorubicin was quantitified by resuspending the nuclei, measuring the associated doxorubicin fluorescence, and relating the doxorubicin fluorescence to doxorubicin mass with the aid of a standard curve. Total mass of dox was divided by the total number of nuclei in suspension, as determined using a Syto staining and a nuclear standard curve, to calculate the total mass of drug per nucleus. For quantifying the mass of aqueous, freely soluble doxorubicin, cells were hypotonically burst by placing them in ddH_2O for 20 min. After the burst, insoluble cell debris was separated by centrifugation at 1,000 × g, with freely soluble doxorubicin released in the supernatant. For measurement of aqueous doxorubicin, supernatants had to be pooled and concentrated by lyophilization, because the mass of free drug was very small.

Binding Assay

Intact cells and isolated nuclei were pulsed for 2 h with 100 nM–500 μM dilutions of doxorubicin in RPMI. After the pulse, nuclei from viable cells were isolated by extraction with 1% Triton X-100 in intracellular buffer, centrifuging the nuclei at 1,000 rpm. Nuclear pellets were washed twice in intracellular buffer. The pellet was then resuspended and total mass of nuclear-associated doxorubicin measured. Dose-dependent binding relationships were analyzed by non-linear curve fitting with SigmaPlot software (Systat, Point Richmond, CA).

Plasmids and Transfection

GFP–VPS4a EQ and KQ constructs were gifts from Dr. Wesley Sundquist (University of Utah, Salt Lake City, UT). K562 cells were plated at a density of 4×10^5 cells/ml in 25 cm^2 cell culture flasks the day of transfection. Cells were transfected using Lipofectamine 2000 (Invitrogen, Carlsbad, CA) according to the manufacturer's protocol 24 h prior to analysis.

Nuclear Efflux from Transfected Cells

Transfected cells were pulsed with 100 μM doxorubicin for 2 h, and then chased in drug-free medium for up to 8 h. To measure nuclear doxorubicin fluorescence, cells were extracted with 0.1% Triton in intracellular buffer for 15 min and then washed with fresh intracellular buffer. Images were acquired with the epifluorescence microscope, and the doxorubicin fluorescence intensities of background-subtracted images were quantified by manually outlining the nuclear perimeter so as to measure the average pixel intensity associated with each nuclear region. For cell population analysis, the cells were binned into percentiles, according to their nuclear intensities. The frequency for each percentile was normalized with the highest frequency value for each cell population set to 1.

Statistical Analysis

The mean and S.E.M. for each experiment was calculated from three separate experiments. To determine statistical significance, a one-tailed homoscedastic *t*-test was performed to calculate the P value.

RESULTS

Evidence that a Physiological Mechanism Facilitates Doxorubicin Efflux from the Cell's Nucleus

First, the rate of doxorubicin efflux from isolated nuclei was compared to the rate of efflux from nuclei in living cells. K562 cells were pulsed with doxorubicin and then chased for up to 8 h in drug-free medium to allow for drug efflux. For comparison, some samples were extracted with detergent immediately after the drug pulse, and the extracted nuclei were incubated in drug-free buffer for 8 h. We found that doxorubicin unbinding from nuclei in living cells was faster than from the corresponding detergent-extracted nuclei (Fig. 1A). After 8 h of efflux, drug content in nuclei of living cells was 44% lower than at the beginning of efflux. In comparison, the drug content in isolated nuclei was only 29% lower.

Doxorubicin Unbinding from Nuclei Occurs in the Presence of Intracellular Doxorubicin at High Concentrations

Remarkably, egress of doxorubicin from nuclei in living cells occurs readily, although a significant amount of doxorubicin remains inside the cell. Doxorubicin was detected fluorometrically, after cells were burst in hypotonic media and then incubated in detergent containing buffer to permeabilize cells and extract all membranes and proteins. As controls, we

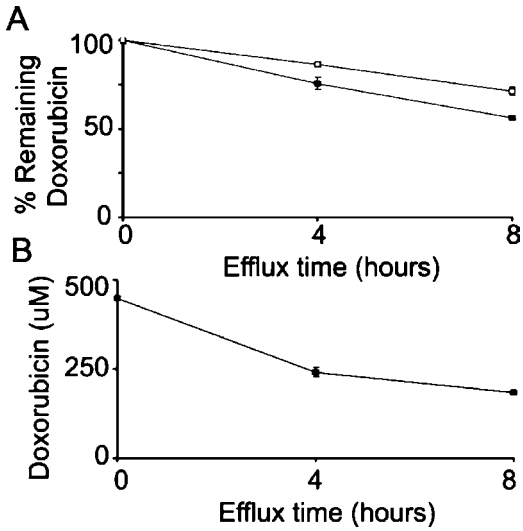

Fig. 1. Efflux of doxorubicin from the nucleus occurs more rapidly in living cells than from isolated nuclei, despite high intracellular drug concentration. (A) The percent of nuclear doxorubicin remaining in living cells (*solid squares*) and isolated nuclei (*open squares*) during the efflux period, measured biochemically. The drug mass per isolated nuclei was significantly higher ($p < 0.005$; *t*-test) than in the nuclei from viable cells after 4 and 8 h of efflux. (B) The total cellular doxorubicin concentrations during the efflux period, measured biochemically. The loss of drug after 4 and 8 h of efflux was significant ($p < 0.005$; *t*-test). Data are the means of three experiments ± S.E.M.

directly established mass balance between the doxorubicin missing from cells and the drug measured in the extracellular medium (data not shown). Also, doxorubicin fluorescence was minimally affected by DNase and proteinase K digestions (data not shown), indicating that the fluorescence signal could be used as an indicator of drug mass. Measuring total drug mass within the cells immediately after the pulse, there were 0.0017 pmol of doxorubicin per cell. Of this, 0.0010 pmol were present in association with each nucleus. During efflux, total cellular doxorubicin decreased gradually, at a rate of ~6% (0.0001 pmol) per hour. Using an estimation of K562 cell volume of 4000 μm^3 (26), the intracellular concentration of drug was 450 μM immediately following the 100 μM drug pulse, and it decreased gradually at ~7% per hour (Fig. 1B) during the efflux period. Thus, not only is doxorubicin concentrated inside the cell relative to the extracellular medium, but most importantly, doxorubicin dissociates from the nucleus even though the intracellular doxorubicin concentration remains higher than the extracellular concentration used to pulse the cells.

Cytoplasmic Doxorubicin is Mostly Associated with Membranous Vesicles and Becomes Increasingly Sequestered during Efflux

Fluorescence microscopy was used to image cells after 0, 4 and 8 h under efflux conditions (Fig. 2A). The intensity of doxorubicin fluorescence in the nucleus became increasingly dim over time as compared to the cytoplasm. The decrease in nuclear doxorubicin fluorescence paralleled the decrease in the mass of doxorubicin in the nucleus, measured biochemically. In the cytoplasm, doxorubicin fluorescence was localized in vesicles, which became more numerous and bright during the course of the efflux period.

To confirm that doxorubicin fluorescence was associated with organelles, GFP was used as a cytosolic marker. K562 cells were transfected with GFP vector, and confocal microscopy was used to visualize GFP and doxorubicin fluorescence accumulating in different parts of the cell (Fig. 2B). To measure the fraction of freely soluble cellular doxorubicin, cells were placed in water to induce cells to swell and burst, allowing exit of freely soluble drug from the cell. The hypotonic burst method not only released the freely soluble doxorubicin from the cytosol, but also released any soluble drug trapped in vesicles, as well as doxorubicin that became unbound during the isolation period. Thus, any measure of doxorubicin released would overestimate the amount of drug actually present in the cytosol of cells. Despite these caveats, the amount of free drug in the cytosol was determined to be less than 10% of the total cellular doxorubicin (Fig 2C). In comparison, the mass of drug released by detergent extraction was approximately 47% of the total doxorubicin per cell, consistent with most of the cytosolic doxorubicin being associated with or trapped by membranes.

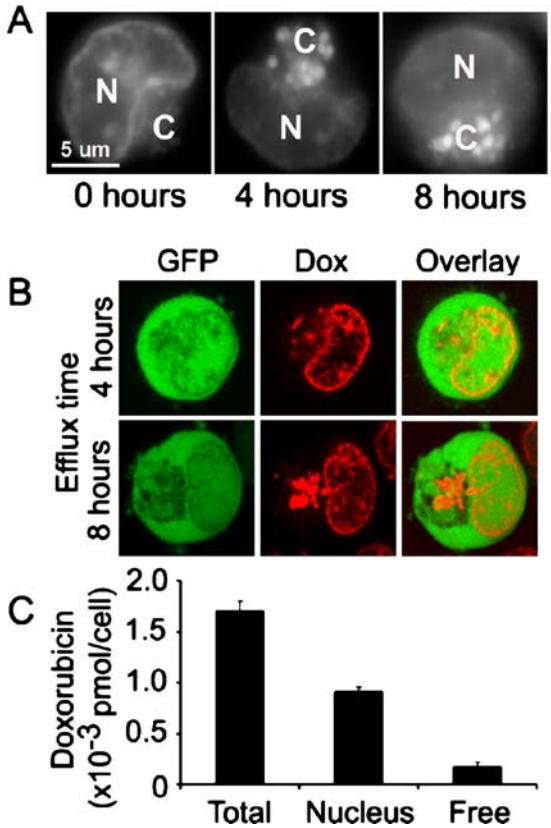

Fig. 2. Cytoplasmic doxorubicin becomes increasingly sequestered in vesicles during efflux. (A) Fluorescence microscopy images of K562 cells after 0, 4, and 8 h efflux periods. The *N* denotes the nucleus, and the *C* denotes the cytoplasmic region. (B) Confocal microscopy images of cells transfected with a GFP vector and then pulsed with doxorubicin after 4 (*top row*) and 8 h (*bottom row*) efflux. The *left column* shows GFP distribution. The *middle column* shows doxorubicin localization. The *right column* is an overlay of these two images. (C) The mass of doxorubicin per cell in different subcellular fractions at the end of the pulse period.

Cytoplasmic Sequestration of Doxorubicin does not Hinder Nuclear Access or Affect the Total Number of Binding Sites, But May Affect the Apparent Affinity of Doxorubicin for DNA

The nuclear volume of K562 cells is approximately 500 μm^3, based on our microscopic observation and previous findings (27). Accordingly, doxorubicin concentration in the nucleus was 1.8 mM immediately following a 100 μM doxorubicin pulse (Fig. 3A). The apparent binding affinities for doxorubicin and DNA in living cells and isolated nuclei were established after incubating cells and isolated nuclei with varying concentration of doxorubicin (Fig. 3B). The dose-binding data was fit using a one-site saturation equation of $y = [B_{Max} * x]/[K_D + x]$. At saturation, maximal binding was 0.0054 pmol of doxorubicin per nucleus in living cells and 0.0055 pmol in isolated nuclei. Approximately, this corresponds to one molecule of doxorubicin for every three base pairs of DNA, consistent with previous results (28). In living cells, half-saturation was achieved when the extracellular concentration was 107 μM (32 μM in isolated nuclei). For both viable cells and isolated nuclei, steady-state concentrations of drug in the nucleus were achieved within 5 min of pulse time (Fig. 3C). Thus, doxorubicin rapidly reaches steady state nuclear concentration without being significantly hindered by the plasma membrane, the nuclear envelope, or by sequestration in cytoplasmic vesicles.

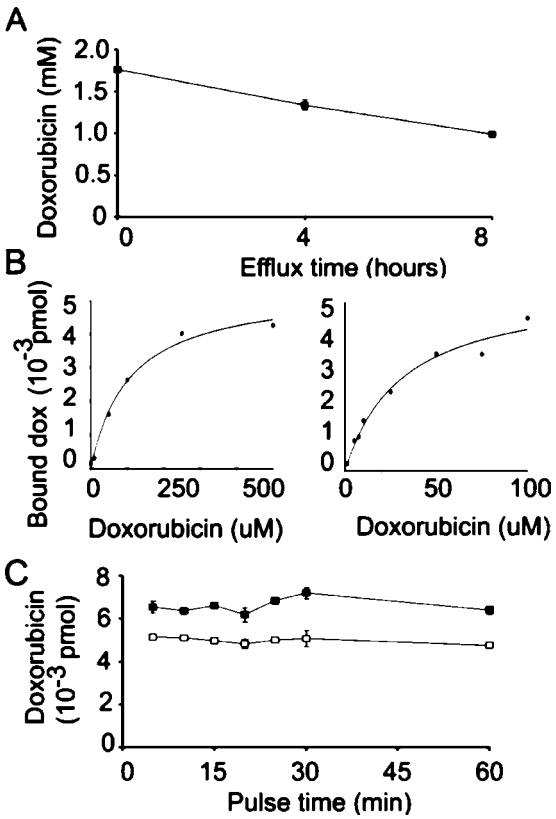

Fig. 3. Doxorubicin transport into and out of extracted and live cell nuclei can be quantitatively analyzed. (A) The nuclear doxorubicin concentration during efflux. The loss of drug from the nucleus after 4 and 8 h of efflux was significant ($p < 0.005$; *t*-test). (B) Mass of doxorubicin in nuclei of living cells (*left graph*) and isolated nuclei (*right graph*) pulsed with doxorubicin at different concentrations. Data are the means of three experiments ± S.E.M. (C) Nuclear doxorubicin values for living cells (*solid squares*) and isolated nuclei (*open squares*) after different doxorubicin pulse times.

Doxorubicin Accumulates in VPS4a Positive Compartments during Efflux

Studying the ultrastructure of K562 cells with electron microscopy, MVBs were the most prominent endo-lysosomal organelles (Fig. 4). Typically, the K562 cell nucleus was kidney-shaped and positioned eccentrically, with the convex surface of the nucleus near the cell surface (Fig. 4A). The distribution of organelles in K562 cells was typically organized in a radial pattern about the center of the cell, with the nucleus to one side and the endoplasmic reticulum and endo-lysosomal organelles at the other. MVBs congregated in the center of the cell. Endoplasmic reticulum tubules were present surrounding the MVBs, and mitochondria were generally localized at the periphery, adjacent to the plasma membrane (Fig. 4B). At high magnification, MVBs were clearly visible as vesicles 500 nm to 1 μm in diameter (Fig. 4C, D). MVBs were replete with smaller vesicles (exosomes), 50 to 80 nm in diameter, and in a few cells, early MVBs with budding exosomes were evident (Fig. 4C). In most cells, lysosomes were not observed. Thus, the bright, doxorubicin-labeled vesicles observed with the fluorescence microscope corresponded in size, shape, number and position to MVBs seen with the electron microscope.

To directly probe if MVBs were involved in doxorubicin sequestration, K562 cells were transfected with GFP-tagged VPS4a EQ and KQ dominant negative mutants to label the MVB. Transfected cells were pulsed and then chased in drug-free media for up to 8 h. Confocal microscopy was used to image VPS4a–GFP and doxorubicin fluorescence. At the beginning of the efflux period, doxorubicin fluorescence was not present in VPS4a-positive vesicles. Nevertheless, after 8 h efflux, doxorubicin fluorescence was mostly present in vesicles that were brightly labeled with VPS4a–GFP fluorescence at their surface (Fig. 5). Doxorubicin fluorescence was clearly visible in the center, surrounded by a ring of VPS4a–GFP in the cytosolic face of the vesicles.

VPS4a Dominant Negatives Decrease Vesicular Sequestration of Drug, However Nuclear Efflux of Drug Can Still Occur

Observing the intracellular distribution of doxorubicin fluorescence in cells expressing dominant-negative VPS4a–GFP revealed a marked decrease in vesicular sequestration in transfected cells (Fig. 6). Counting visible doxorubicin-containing vesicles with a diameter greater than 0.5 μm, we found that cells transfected with VPS4a EQ and KQ dominant negatives exhibited on average four and three doxorubicin vesicles per cell, respectively; control vector-transfected and untransfected cells contained more than ten vesicles per cell (Fig. 6B). To determine if this decrease in doxorubicin-labeled vesicles reflected a decrease in doxorubicin efflux from the nucleus, cells transfected with VPS4a-EQ were pulsed-chased with doxorubicin, and extracted with 0.1% Triton X-100 which removes cytoplasmic doxorubicin fluores-

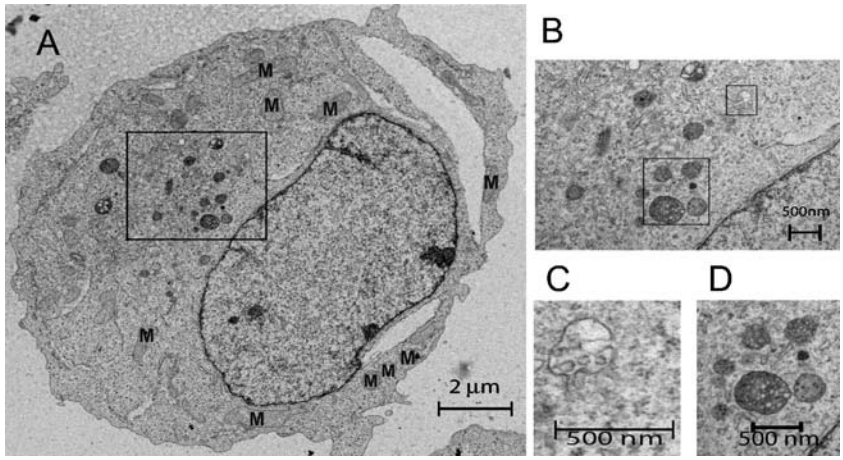

Fig. 4. The MVB is the most prominent endo-lysosomal compartment in K562 cells. (A) Electron micrograph (5,800× magnification) of a K562 cell. Some mitochondria are labeled with an "M" to distinguish them from the MVBs. (B) Magnification (13,500×) of MVBs present in clusters in the cytoplasm in the *center* of the cell. MVBs showing early (C) and more mature (D) morphologies.

cence but does not completely extract dominant negative VPS4a–GFP labeling. Images were acquired using a fluorescence microscope after 0 and 8 h chase periods, and the intensity of doxorubicin fluorescence in the nuclei was compared using image analysis software. After 8 h of efflux, the intensity of nuclear doxorubicin fluorescence decreased to a similar extent in both untransfected cells and those expressing the VPS4a EQ dominant negative mutant (Fig. 7A). Cell population analysis of fluorescence intensity distribution was consistent with doxorubicin efflux from the nucleus occurring at similar rates in transfected and control cells (Fig. 7B). The nuclear fluorescence labeling for both groups exhibited a standard distribution about the mean fluorescence, and the mean fluorescence shift was accompanied by a shift of the entire population.

DISCUSSION

Consistent with previous results (29), the rate of doxorubicin egress from isolated nuclei is slow (3% per hour), which allows for the measurement of the doxorubicin mass that remains associated with isolated nuclei. The rate of drug efflux from nuclei in living cells occurs more rapidly (Fig. 1A). This faster rate suggests an active cellular mechanism facilitating efflux of doxorubicin from the nucleus. High intracellular concentrations of drug are present as nuclear efflux is occurring (Fig. 1B). Although the apparent affinity of doxorubicin for nuclei is less in living cells than in isolated nuclei (Fig. 3B), unbinding of doxorubicin from living cells occurs in the presence of intracellular drug concentrations higher than the concentration used to pulse the cells. Our data suggests that sink conditions are present in the intact cell despite a large amount of intracellular doxorubicin, indicating that much of the cellular doxorubicin is not in a free form that can interact with DNA.

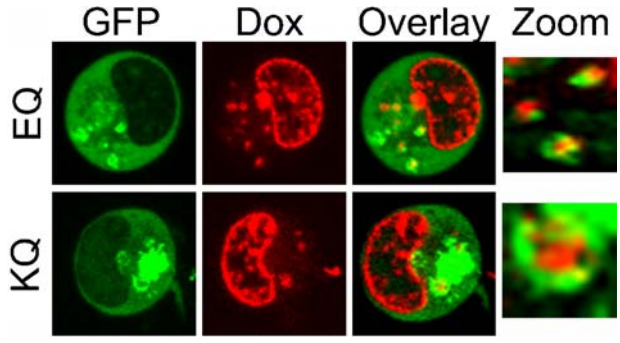

Fig. 5. Doxorubicin accumulates in VPS4a positive vesicles. Confocal microscopy images of K562 cells transfected with GFP–VPS4a EQ (*top row*) or KQ (*bottom row*) dominant negative mutants after 8 h efflux. The *far left column* shows GFP–VPS4a EQ or KQ distribution. The *second column* shows doxorubicin localization. The *third column* is an overlay of the two images. The *far right column* is a magnification of cytoplasmic vesicles with GFP–VPS4a EQ or KQ (*green*) encircling doxorubicin fluorescence (*red*).

Thus, we infer that most of the cellular doxorubicin must be compartmentalized in a manner that allows unbinding from DNA to occur despite a high intracellular drug concentration. Microscopic analysis of doxorubicin localization reveals most of the cytoplasmic doxorubicin fluorescence associated with vesicles (Fig. 2A). The divergent localization of doxorubicin fluorescence and GFP, an aqueous marker of the cytosol, is evidence of doxorubicin fluorescence being present in a non-cytosolic cytoplasmic compartment (Fig. 2B). Hypotonic burst of cells renders them permeant to Trypan Blue, a molecule larger than doxorubicin (data not shown). Thus, all freely soluble doxorubicin molecules should be released. Experimentally, only a small fraction (<10%) of the total cellular doxorubicin is released after such hypotonic burst (Fig. 2C).

While most of the doxorubicin remaining in the cell after extracellular drug is removed remains trapped or bound to membranous vesicles, vesicular sequestration, by trapping or sequestration or a combination of the two, does not seem to stop doxorubicin from reaching the nucleus. Because doxorubicin readily interacts with the nucleus in the influx experiment, we infer that there is a significant amount of free doxorubicin present in the cell when cells are in the presence of extracellular drug. However, when doxorubicin is removed from the extracellular medium, our data suggests there is a depletion of free drug from cells, either through intracellular

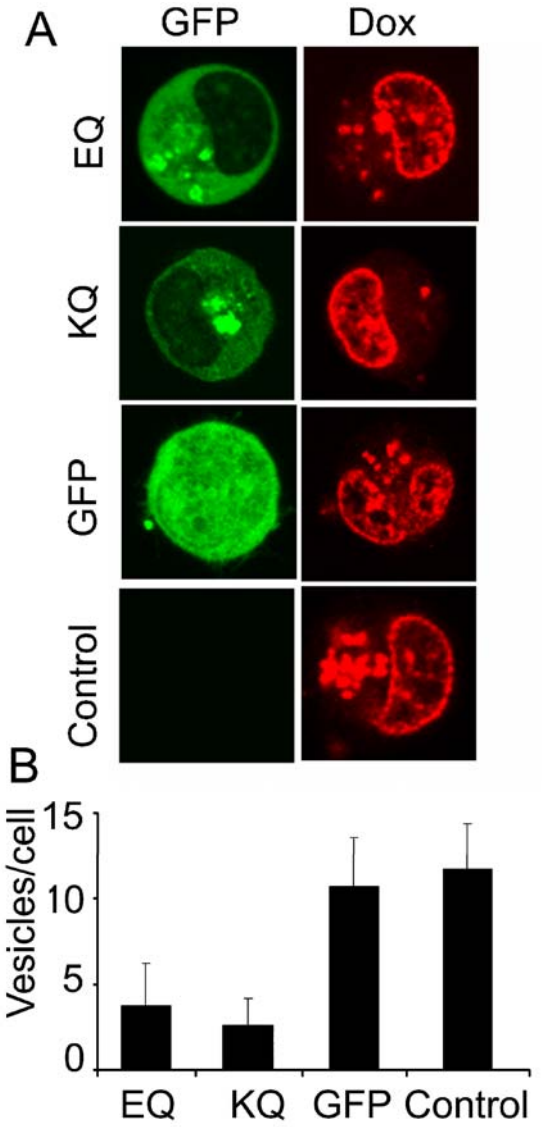

Fig. 6. VPS4a dominant negatives decrease doxorubicin-positive vesicles. (A) Confocal microscopy images of untransfected cells, and cells transfected with GFP–VPS4a EQ, GFP–VPS4a KQ, or the GFP vector alone, after 8 h efflux. The *left column* shows the fluorescence of GFP-tagged VPS4a dominant negative mutants and GFP alone. The *right column* shows doxorubicin fluorescence. (B) The number of doxorubicin-containing vesicles in cells transfected with VPS4a dominant negative mutants, and control cells ($n \geq 10$).

sequestration, through efflux across the plasma membrane or both. Still, a large amount of doxorubicin remains inside the cell, but most of it is bound. Membrane extraction with detergent releases ~46% of the cellular doxorubicin, with the rest remaining bound to the nucleus. Most likely, the doxorubicin that remains bound to the nucleus is associated with DNA. We have established that the stoichiometry of doxorubicin binding to nuclei corresponds to the stoichiometry of doxorubicin binding to DNA (i.e., one doxorubicin molecule for every three base pairs of DNA).

In K562 cells, the plasma membrane does not pose a significant barrier to drug entry, as intracellular drug concentrations are more than four times greater than the extracellular concentration at the end of the pulse. The nuclear membrane does not hinder drug entry either, which is to be expected given that the nuclear pore complex allows for the passive diffusion of molecules smaller than 9 nm in diameter (30). Concentration of doxorubicin in the nucleus is even greater (Fig. 3A) reaching steady state within a 5-min drug pulse (Fig. 3C). In contrast, sequestration of drug in cytoplasmic vesicles occurs more gradually, so sequestration does not prevent nuclear entry.

With electron microscopy, MVBs can be seen as the most prominent and abundant endolysosomal compartment in K562 cells (Fig. 4). Based on the size, shape, and subcellular localization of MVBs, we infer that they correspond to the major site of vesicular doxorubicin sequestration in K562 cells. Unlike lysosomes, MVBs contain large numbers of internal vesicles produced from invaginations that form on the outer membrane of the MVB, in a process that resembles the budding of viruses (24). In other somatic cells, MVB formation is the mechanism through which mono-ubiquitinated transmembrane proteins and receptors are sorted into exosomes and shuttled to the lysosomes for degradation (31). In cells of erythroid lineage, such as K562 cells, the inner vesicles of the MVB are not degraded intracellularly, but are released to the outside of the cell after fusion of MVBs with the plasma membrane (32).

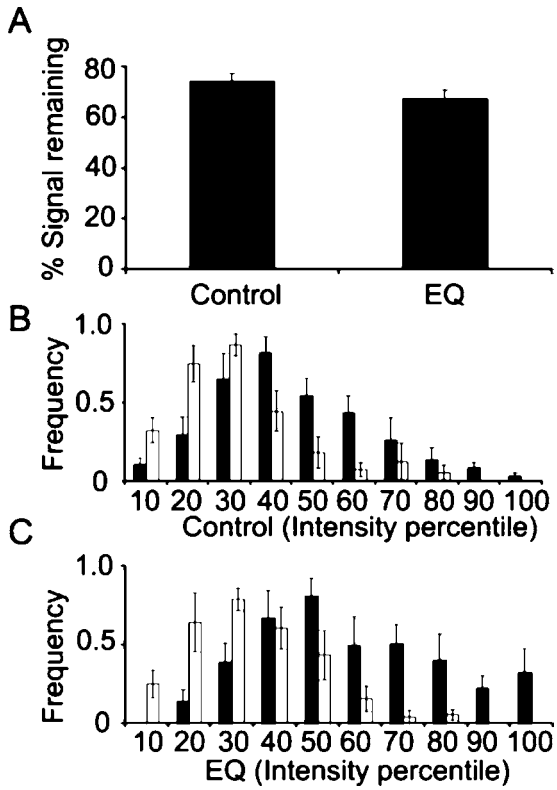

Fig. 7. Nuclear efflux of control and dominant negative VPS4a expressing cells is similar. (A) Average nuclear intensity of cells transfected with VPS4a EQ and untransfected cells after 8 h efflux. There was no significant difference in nuclear doxorubicin intensity between transfected and control cells ($p > 0.2$; *t*-test). (B) Frequency of untransfected (*top graph*) and transfected (*bottom graph*) cells exhibiting a given average intensity percentile after 0 (*solid bars*) and 8 h (*open bars*) of efflux. Data are means of three experiments with more than 80 cells analyzed in each experiment.

To assess whether the MVB-exosome pathway facilitates doxorubicin clearance from the nucleus, K562 cells were transfected with GFP-tagged VPS4a dominant negative mutants (24,25). Dominant negative VPS4a binds to MVBs, slowing down endosomal trafficking and exosome release and leading to the formation of an enlarged MVB compartment known as the class E compartment (33). Under efflux conditions, doxorubicin fluorescence accumulated in the VPS4a-positive compartment over the course of 8 h (Fig. 5), consistent with drug molecules trafficking through the MVB on their way out of the cell.

Expression of VPS4a dominant negatives appeared to decrease the total amount of doxorubicin fluorescence observed in cytoplasmic vesicles, but did not prevent the decrease of nuclear doxorubicin fluorescence during the 8-h efflux period (Fig. 6). Thus, although interfering with VPS4a function may inhibit doxorubicin sequestration or trafficking through the MVB, it did not appear to affect drug egress from the nucleus (Fig. 7). This was an unexpected result. A likely explanation is that because drug efflux is ultimately driven by the concentration gradient between the nucleus and the outside of the cell, drug egress from the nucleus occurs through an alternative pathway when the MVB-exosome efflux pathway is blocked. We did not observe an increase in the intensity of doxorubicin fluorescence associated with individual vesicles. On the other hand, doxorubicin can interact with other membranous organelles inside the cell, such as mitochondria, the endoplasmic reticulum, and intracellular vesicles expressing drug transporter proteins. Binding to proteins that are actively exported from the nucleus to the cytoplasm may facilitate nuclear efflux (34). In this context, the proteasome has been proposed to facilitate translocation of doxorubicin from the nucleus to the cytosol (35). Thus, blocking the MVB pathway could simply increase the amount of doxorubicin efflux along this alternative pathway.

In conclusion, doxorubicin transport occurs in two different steps: first, DNA-bound drug molecules dissociate from DNA; second, drug molecules gradually make their way out of the cell. The route of doxorubicin egress from the nucleus to the extracellular medium is facilitated by a cellular mechanism, involving the MVB, but is not necessarily constrained to the MVB pathway. If MVB traffic is blocked, doxorubicin molecules may still exit the nucleus through a different route. Just like damming a river midstream, dominant negative VPS4a do not necessarily alter the flow of molecules upstream, and perturbing drug transport in the cytoplasm is not necessarily sufficient to prevent nuclear efflux from happening in the first place.

ACKNOWLEDGMENTS

We thank Wesley Sundquist for the GFP–VPS4a EQ and KQ constructs. This work was supported by a grant from the National Institutes of Health (CA104686, G.R.R.). V.Y.C. was supported by a Pre-Doctoral Fellowship from the Pharmaceutical Research and Manufacturers of America Foundation and a Pharmacological Sciences Training Grant from the National Institute of General Medical Sciences (GM07767). Contents are solely the responsibility of the authors and do not necessarily represent the official views of NIGMS.

REFERENCES

1. M. M. Gottesman. Mechanisms of cancer drug resistance. *Annu. Rev. Med.* **53**:615–627 (2002).
2. G. Chang. Multidrug resistance ABC transporters. *FEBS Lett.* **555**:102–105 (2003).
3. A. K. Larsen, A. E. Escargueil, and A. Skladanowski. Resistance mechanisms associated with altered intracellular distribution of anticancer agents. *Pharmacol. Ther.* **85**:217–229 (2000).
4. M. J. Van Luyn, M. Muller, J. Renes, C. Meijer, R. J. Scheper, E. F. Nienhuis, N. H. Mulder, P. L. Jansen, and E. G. De Vries. Transport of glutathione conjugates into secretory vesicles is mediated by the multidrug-resistance protein 1. *Int. J. Cancer* **76**:55–62 (1998).
5. A. Rajagopal and S. M. Simon. Subcellular localization and activity of multidrug resistance proteins. *Mol. Biol. Cell* **14**:3389–3399 (2003).
6. A. B. Shapiro, K. Fox, P. Lee, Y. D. Yang, and V. Ling. Functional intracellular P-glycoprotein. *Int. J. Cancer* **76**: 857–864 (1998).
7. D. A. Gewirtz. A critical evaluation of the mechanisms of action proposed for the antitumor effects of the anthracycline antibiotics adriamycin and daunorubicin. *Biochem. Pharmacol.* **57**:727–741 (1999).
8. J. A. Endicott and V. Ling. The biochemistry of P-glycoprotein-mediated multidrug resistance. *Annu. Rev. Biochem.* **58**:137–171 (1989).
9. S. P. Cole, G. Bhardwaj, J. H. Gerlach, J. E. Mackie, C. E. Grant, K. C. Almquist, A. J. Stewart, E. U. Kurz, A. M. Duncan, and R. G. Deeley. Overexpression of a transporter gene in a multidrug-resistant human lung cancer cell line. *Science* **258**:1650–1654 (1992).
10. Y. Gong, M. Duvvuri, and J. P. Krise. Separate roles for the Golgi apparatus and lysosomes in the sequestration of drugs in the multidrug-resistant human leukemic cell line HL-60. *J. Biol. Chem.* **278**:50234–50239 (2003).
11. J. E. Gervasoni Jr, S. Z. Fields, S. Krishna, M. A. Baker, M. Rosado, K. Thuraisamy, A. Hindenburg, and R. N. Taub. Subcellular distribution of daunorubicin in P-glycoprotein-positive and -negative drug-resistant cell lines using laser-assisted confocal microscopy. *Cancer Res.* **51**:4955–4963 (1991).
12. M. A. Sognier, Y. Zhang, R. L. Eberle, K. M. Sweet, G. A. Altenberg, and J. A. Belli. Sequestration of doxorubicin in vesicles in a multidrug-resistant cell line (LZ-100). *Biochem. Pharmacol.* **48**:391–401 (1994).
13. C. Bour-Dill, M. P. Gramain, J. L. Merlin, S. Marchal, and F. Guillemin. Determination of intracellular organelles implicated in daunorubicin cytoplasmic sequestration in multidrug-resistant MCF-7 cells using fluorescence microscopy image analysis. *Cytometry* **39**:16–25 (2000).
14. P. Ferrao, P. Sincock, S. Cole, and L. Ashman. Intracellular P-gp contributes to functional drug efflux and resistance in acute myeloid leukaemia. *Leuk. Res.* **25**:395–405 (2001).
15. C. M. Fader, A. Savina, D. Sanchez, and M. I. Colombo. Exosome secretion and red cell maturation: exploring molecular components involved in the docking and fusion of multivesicular bodies in K562 cells. *Blood Cells Mol. Diseases* **35**:153–157 (2005).
16. A. Savina, M. Vidal, and M. I. Colombo. The exosome pathway in K562 cells is regulated by Rab11. *J. Cell Sci.* **115**:2505–2515 (2002).
17. A. Savina, M. Furlan, M. Vidal, and M. I. Colombo. Exosome release is regulated by a calcium-dependent mechanism in K562 cells. *J. Biol. Chem.* **278**:20083–20090 (2003).
18. S. Simon, D. Roy, and M. Schindler. Intracellular pH and the control of multidrug resistance. *Proc. Natl. Acad. Sci. USA* **91**: 1128–1132 (1994).
19. R. Safaei, B. J. Larson, T. C. Cheng, M. A. Gibson, S. Otani, W. Naerdemann, and S. B. Howell. Abnormal lysosomal trafficking and enhanced exosomal export of cisplatin in drug-resistant human ovarian carcinoma cells. *Mol. Cancer Ther.* **4**:1595–1604 (2005).
20. K. Shedden, X. T. Xie, P. Chandaroy, Y. T. Chang, and G. R. Rosania. Expulsion of small molecules in vesicles shed by cancer

cells: association with gene expression and chemosensitivity profiles. *Cancer Res.* **63**:4331–4337 (2003).
21. M. Babst, T. K. Sato, L. M. Banta, and S. D. Emr. Endosomal transport function in yeast requires a novel AAA-type ATPase, Vps4p. *Embo J.* **16**:1820–1831 (1997).
22. M. Babst, B. Wendland, E. J. Estepa, and S. D. Emr. The Vps4p AAA ATPase regulates membrane association of a Vps protein complex required for normal endosome function. *Embo J.* **17**: 2982–2993 (1998).
23. S. Scheuring, R. A. Rohricht, B. Schoning-Burkhardt, A. Beyer, S. Muller, H. F. Abts, and K. Kohrer. Mammalian cells express two VPS4 proteins both of which are involved in intracellular protein trafficking. *J. Mol. Biol.* **312**:469–480 (2001).
24. J. E. Garrus, U. K. von Schwedler, O. W. Pornillos, S. G. Morham, K. H. Zavitz, H. E. Wang, D. A. Wettstein, K. M. Stray, M. Cote, R. L. Rich, D. G. Myszka, and W. I. Sundquist. Tsg101 and the vacuolar protein sorting pathway are essential for HIV-1 budding. *Cell* **107**:55–65 (2001).
25. N. Bishop and P. Woodman. ATPase-defective mammalian VPS4 localizes to aberrant endosomes and impairs cholesterol trafficking. *Mol. Biol. Cell* **11**:227–239 (2000).
26. E. Klein, H. Ben-Bassat, H. Neumann, P. Ralph, J. Zeuthen, A. Polliack, and F. Vanky. Properties of the K562 cell line, derived from a patient with chronic myeloid leukemia. *Int. J. Cancer* **18**:421–431 (1976).
27. R. Hancock. A role for macromolecular crowding effects in the assembly and function of compartments in the nucleus. *J. Struct. Biol.* **146**:281–290 (2004).
28. A. Rabbani, M. Iskandar, and J. Ausio. Daunomycin-induced unfolding and aggregation of chromatin. *J. Biol. Chem.* **274**: 18401–18406 (1999).
29. M. Duvvuri, W. Feng, A. Mathis, and J. P. Krise. A cell fractionation approach for the quantitative analysis of subcellular drug disposition. *Pharm. Res.* **21**:26–32 (2004).
30. P. L. Paine, L. C. Moore, and S. B. Horowitz. Nuclear envelope permeability. *Nature* **254**:109–114 (1975).
31. D. J. Katzmann, M. Babst, and S. D. Emr. Ubiquitin-dependent sorting into the multivesicular body pathway requires the function of a conserved endosomal protein sorting complex, ESCRT-I. *Cell* **106**:145–155 (2001).
32. R. M. Johnstone, A. Mathew, A. B. Mason, and K. Teng. Exosome formation during maturation of mammalian and avian reticulocytes: evidence that exosome release is a major route for externalization of obsolete membrane proteins. *J. Cell Physiol.* **147**:27–36 (1991).
33. C. K. Raymond, I. Howald-Stevenson, C. A. Vater, and T. H. Stevens. Morphological classification of the yeast vacuolar protein sorting mutants: evidence for a prevacuolar compartment in class E vps mutants. *Mol. Biol. Cell* **3**:1389–1402 (1992).
34. T. A. Chan, H. Hermeking, C. Lengauer, K. W. Kinzler, and B. Vogelstein. 14-3-3 Sigma is required to prevent mitotic catastrophe after DNA damage. *Nature* **401**:616–620 (1999).
35. K. Kiyomiya, S. Matsuo, and M. Kurebe. Mechanism of specific nuclear transport of adriamycin: the mode of nuclear translocation of adriamycin–proteasome complex. *Cancer Res.* **61**: 2467–2471 (2001).